>20% Efficient 80 µm Thin Industrial-Type Large-Area Solar Cells from 100 µm Sawn c-Si Wafers

Yvonne Schiele, Nils Brinkmann*, Jan Ebser, Renate Horbelt, Alexander Frey, Josh Engelhardt, Giso Hahn, and Barbara Terheiden

University of Konstanz, Department of Physics, P.O. Box 676, D-78457 Konstanz, Germany

Abstract — **Reducing the thickness of crystalline Si wafers to be processed into solar cells yields several significant benefits: PV module manufacturing cost can be reduced and the required diffusion length of minority carriers is smaller. The latter in turn enables a higher efficiency potential and a larger spread of Si materials to be employed for rear junction solar cell concepts which are advantageous for n-type devices. Industrial-type 80 µm thin large-area rear junction solar cells manufactured from 100 µm wire-sawn wafers exhibit an independently certified efficiency of 20.1% with V_{OC} of 672 mV.**

Index Terms — **boron, n-type, photovoltaic cells, selective, silicon, thin wafers.**

* now with Solexel Inc., Milpitas, USA

I. Introduction

About 40% of the crystalline Si PV module manufacturing cost is occasioned by the required Si feedstock, crystal growing and wafering, i.e. the Si wafer [1]. Hence, as recent research efforts of prominent solar companies have shown [2-4], reducing wafer thickness of c-Si solar cells is an opportunity to substantially decrease the cost per watt-peak of PV. In [5], an average wafer thickness of 100 µm in already <10 years is predicted.

Within the European project "20 percent efficiency on less than 100 µm thick industrially feasible crystalline silicon solar cells (20plµs)", the entire process chain for thin solar cells, from wafering to module integration, has been studied [6].

Instead of saving material cost either by using Si ribbon [7], which in general provides lower electronic quality, or by employing a challenging Si epitaxy process [4], in this study, the well-engineered standard Czochralski (Cz) growth process from Si feedstock is utilized.

Recently announced efficiencies of thin c-Si solar cells are usually achieved on wafers thinned after sawing. Within the "20plµs" project, wire-sawing technology has been advanced to direct slicing wafer thicknesses of 100 µm being half the thickness of today's standard with due regard to low breakage rate, surface roughness, and high thickness uniformity [6,8].

Aside from the cost savings, the physical advantage of thinner wafers consists in the higher V_{OC} and efficiency potential provided that surface recombination is low enough [2] and in the smaller required diffusion length of minority carriers in the Si bulk. As it has been simulated [9], thinner wafers enable a broader spread of Si material (different resistivities) to be employed for rear junction solar cell concepts being mainly limited by insufficiently great diffusion lengths. This is also the reason why usually n-type Si is used to manufacture rear junction solar cells since it features a higher tolerance of carrier lifetime to common impurities.

Rear junction solar cell concepts based on n-type Si provide several advantages:

By moving the emitter to the rear, the polarity sequence $n^+ - \text{base} - p^+$ (front to rear) of the n-type solar cell becomes the same as for a standard p-type device; only the base doping type is changed. Therefore, established solar cell components with the corresponding processes can be used:

- At the front, the n^+ doped layer by $POCl_3$ diffusion is employed as a front surface field (FSF). Selective etch-back of the FSF ensures very low recombination activity (saturation current density $j_{0FSF} \approx 30$ fA/cm^2 in the passivated areas [10]) where the main light absorption occurs.
- For front metalization, standard Ag screen-print technology (high aspect ratio, high conductivity, low contact resistivity) can be utilized.
- For the substitution of p-type by such n-type solar cells in an existing industrial high volume production, less investment for new equipment and process adaption effort is required.

As an additional advantage of the rear junction concept, since FSF and Si base have the same polarity, the base contributes to lateral conductivity of the majority electrons. This enables FSF sheet resistance and front finger distance to be chosen greater.

In the investigated solar cell concept, the rear metallization is implemented as a full-area Al (physical vapor deposition) which locally contacts the B emitter through a laser-opened dielectric passivation layer. This may permit less Al spiking than with Ag/Al screen-printed paste while maintaining a low contact resistivity and serves, in combination with the passivation layer underneath, as an effective internal optical rear reflector [11,12] being especially important for thin solar cells to maintain high current density. Additionally, the emitter surface need not be textured in order to maintain low contact resistivity or good adhesion (contrary to a screen-printed Ag/Al grid). This leads to generally lower emitter saturation current density ($\Delta j_{0e} \approx$ 10-20 fA/cm^2 [10]) due to a smaller crystal surface, easier laser ablation of the passivation layer and an enhanced rear reflection.

II. Experimental Details

The solar cell concept investigated within this study is implemented on large-area n-type Cz-Si wafers (125×125 mm^2, wire-sawn to 100 µm thickness, 2 Ωcm resistivity) being processed according to an industry-oriented manufacturing sequence (Fig. 1).

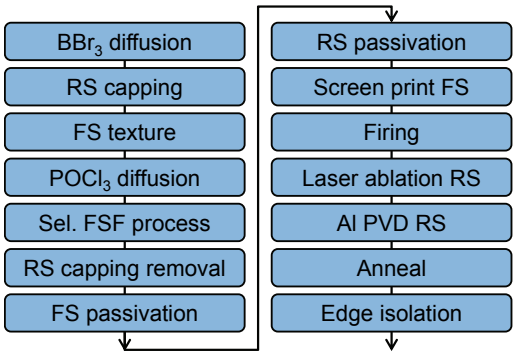

Fig. 1. Processing sequence of the n-type rear junction solar cell.

An initial BBr_3 diffusion after saw damage removal and cleaning creates the B emitter which is capped by SiN_x on the rear. An alkaline texture removes the emitter at the front. Subsequently, the wafers are subjected to a $POCl_3$ diffusion creating the FSF (40 Ω/sq) which is then selectively etched-back (100 Ω/sq) in the non-masked regions between the contact areas (selective FSF process) [13,14]. With the rear capping layer removed, the front surface is passivated by a stack of thermal SiO_2 and SiN_x, the emitter by an Al_2O_3/SiN_x stack. After screen-printing (standard single print) and firing the front Ag grid, the rear passivation is locally opened by means of laser ablation, Al is deposited by electron beam evaporation on the whole area and finally annealed at low temperatures in order to repair the electron beam damage [15] and enhance rear contact.

The cross section of the resulting n-type rear junction solar cell is depicted in Fig. 2.

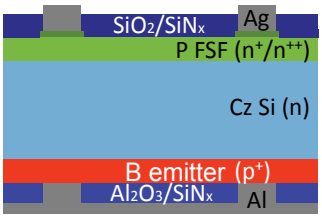

Fig. 2. Cross section of the n-type rear junction solar cell.

To quantify the gain by the selective n^+ structuring and its particular importance to a rear junction device, similar solar cells but with a homogeneous FSF (60 Ω/sq $POCl_3$ diffusion) are manufactured as a reference (cf. sec. IV.*A*).

As a fundamental component of the solar cell, three different B rear emitters (Fig. 3) are applied to the solar cells with sheet resistances R_{sheet} between 35 and 110 Ω/sq whose performance dependencies (recombination activity, contact properties) on emitter characteristics (R_{sheet}, profile depth, surface doping) have been investigated in [16] (cf. sec. IV.*B*).

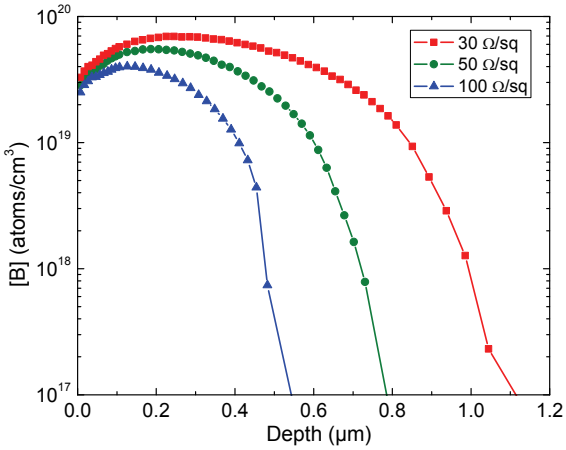

Fig. 3. Profiles of the three BBr_3 emitters as they are in the finished solar cell between the rear contact spots, measured by electrochemical capacitance-voltage (ECV) method.

In order to quantify the loss mechanisms which affect *FF* of the solar cells in greater detail, a fill factor loss analysis (FFLA) is carried out following the approach in [17] (cf. sec. IV.*C*). The individual losses are easily comparable since they are stated in (%$_{abs}$) units. An upper limit of the fill factor (FF_{j01}) disregards the *FF* losses due to R_{series}, R_{shunt} and j_{02} recombination:

$$FF_{j_{01}} = \frac{V_{mpp,\,j_{01}}\, j_{mpp,\,j_{01}}}{V_{OC} j_{SC}} \qquad (1)$$

with $V_{mpp,\,j01}$ and $j_{mpp,\,j01}$ defining the corresponding maximum power point. The *FF* losses due to the resistances are calculated by

$$\Delta FF_{R_{series}} = \frac{j_{mpp}^{\,2} R_{series}}{V_{OC} j_{SC}} \qquad (2)$$

and

$$\Delta FF_{R_{shunt}} = \frac{(V_{mpp} + j_{mpp} R_{series})^2}{R_{shunt} V_{OC} j_{SC}} \,. \qquad (3)$$

The influence of j_{02} recombination is determined by the difference of the j_{01} limit and the resistance-free fill factor $FF_{|R}$

$$\Delta FF_{j_{02}} = FF_{j_{01}} - FF_{|R} \,. \qquad (4)$$

TABLE I
I-V DATA OF THE BEST SOLAR CELL OF EACH EMITTER GROUP (IN-HOUSE MEASUREMENT) AND OF CHAMPION CELL WITH 55 Ω/SQ EMITTER (INDEPENDENTLY CERTIFIED MEASUREMENT)

	Illuminated IV				Multi-light method	Dark IV	2-diode model fit	
Emitter R_{sheet} (Ω/sq)	**V_{OC} (mV)**	**j_{SC} (mA/cm²)**	**FF (%)**	**η (%)**	**R_{series} (Ωcm²)**	**R_{shunt} (kΩcm²)**	**j_{01} (fA/cm²)**	**j_{02} (nA/cm²)**
35	670	38.1	78.3	20.0	0.79	752	111	10.2
55	670	38.0	78.6	20.0	0.76	128	110	11.7
55 (FhG ISE CalLab)	672	37.8	78.9	20.1	-	-	-	-
110	669	38.5	77.0	19.8	0.80	43	85	25.6

III. IV RESULTS

The manufactured 80 µm thin large-area rear junction solar cells with the three different emitters exhibit conversion efficiencies ranging from 19 to 20% (means in Fig. 4, best values in Tab. I). An independently certified measurement (FhG ISE CalLab) of the champion cell featuring a 55 Ω/sq emitter attests an efficiency of $\eta = 20.1\%$, which is to our knowledge the highest value of an 80 µm thin large-area solar cell from a 100 µm wire-sawn wafer announced thus far.

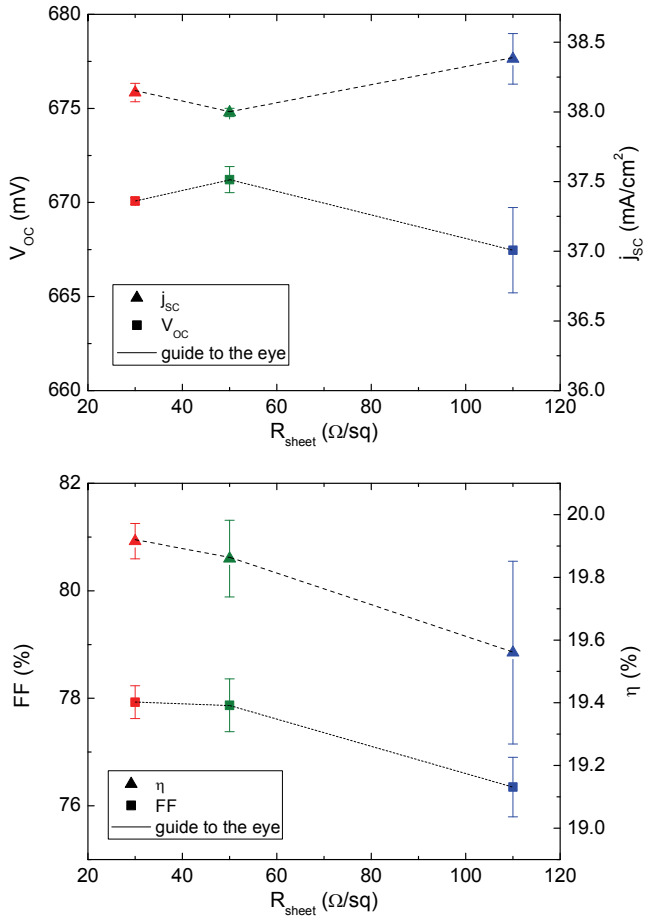

Fig. 4. I-V data mean values of the manufactured 80 µm thin rear junction solar cells for three different emitters (3 cells per group).

All solar cells are characterized by excellent open circuit voltages of $V_{OC} = 664$-672 mV. The values of all individual 35 and 55 Ω/sq samples are very similar (670-672 mV), whereas the individual 110 Ω/sq devices diverge by up to 5 mV.

Short circuit current density is very similar for the two lower-ohmic emitters ($j_{SC} = 38.0$-38.2 mA/cm²) whereas the 110 Ω/sq solar cells attain up to 38.5 mA/cm² which is a noteworthy figure for an 80 µm thin front side screen-printed device.

However, the main cause for the lower efficiency of the high R_{sheet} devices is the significantly lower fill factor of $FF \approx 76$-77% compared to ~78% for the remaining R_{sheet} range. Again, with increasing R_{sheet}, FF of the individual solar cells diverges further. Thus, the similar trend of the efficiency values can be explained.

In section IV, the I-V data of only the best solar cells of each emitter group are chosen to discuss and compare their characteristics in greater detail.

IV. ANALYSIS & DISCUSSION

A. Front Surface Field

The I-V data of the best solar cells with selective and homogeneous FSF (both with 55 Ω/sq emitter) are listed in Tab. II. Saturation current density of the etched-back FSF (100 Ω/sq) is reduced by ~100 fA/cm² to $j_{0FSF} \approx 30$ fA/cm² in the passivated areas compared to the homogeneous FSF (60 Ω/sq) [10]. Therefore, the selective FSF enables a significant V_{OC} and j_{SC} increase by $\Delta V_{OC} = 19$ mV or $\Delta j_{SC} = 2.9$ mA/cm², respectively, compared to a homogeneous FSF. Despite a $1.7\%_{abs}$ FF decrease, the total efficiency gain amounts to $\Delta\eta = 1.6\%_{abs}$. This demonstrates that it is essential for rear junction solar cells to minimize the recombination activity at the front. The beneficial effect of the selectively etched-back FSF is enhanced by combining it with a highly effective passivation as it is implemented by the SiO_2/SiN_x stack in this study.

B. Rear Emitter

Saturation current density j_{02} increases with R_{sheet} (Tab. I) and correspondingly with decreasing emitter depth (Fig. 3). By annealing the solar cells, rear contact Al spikes into the

TABLE II
I-V DATA OF BEST SOLAR CELLS WITH SELECTIVE VS. HOMOGENEOUS FSF (50 Ω/SQ EMITTER)

FSF type	V_{OC} (mV)	j_{SC} (mA/cm²)	*FF* (%)	η (%)
Sel. FSF	670	38.0	78.6	20.0
Hom. FSF	652	35.1	80.3	18.4

space charge region (SCR) which is more pronounced for shallower emitters. Thus, *FF* rises first as the metal/Si contact is enhanced. But after longer annealing, it degrades again during the temperature process. Therefore, the optimal annealing duration has to be adapted to emitter depth.

Hence, the increased j_{02} due to Al spiking into the SCR causes a *FF* reduction mainly of the 110 Ω/sq solar cell (Tab. I). Its lower R_{shunt}, on the other hand, reflects that the spiking does not only affect the SCR but may also locally pierce the emitter and slightly shunt the p/n junction which further reduces *FF*. The *FF* drop of ~1-2%$_{abs}$ may also be induced by the higher series resistance of the low doped emitter (cf. sec. *C*).

Saturation current density j_{01}, however, decreases with increasing R_{sheet} (Tab. I) indicating the high passivation quality of the dielectric stack on the emitter. Otherwise the effect of the electric field of the emitter itself keeping minorities off the surface would predominate and therefore j_{01} would have to diminish with R_{sheet}. j_{01} of the solar cell with 110 Ω/sq emitter is considerably lower compared to the two lower ohmic emitters which is caused by i.a. its significantly diminished j_{0e} in the passivated areas of 19 fA/cm² compared to 28 (55 Ω/sq) and 32 fA/cm² (35 Ω/sq) (induced by the less deep emitter profile) [16]. This yields a higher j_{SC} due to less recombination in the low doped emitter (Tab. I). V_{OC}, however, is similar for all emitters since the expected V_{OC} increase due to the j_{01} reduction is overcompensated by the detrimental effects of Al spiking into the SCR (Tab. I).

C. Fill Factor Loss Analysis

Since the efficiency of the solar cells with the different emitters differs mainly due to the *FF* discrepancies, a detailed fill factor loss analysis (FFLA) is carried out which quantifies the extent to which *FF* is affected by various loss mechanisms. Complementary to the best solar cell of each emitter group ("35 Ω/sq", 55 Ω/sq", 110 Ω/sq$^{(b)}$"), another similarly processed but unequally performing 110 Ω/sq sample ("110 Ω/sq$^{(a)}$") is selected to be analyzed.

The FFLA clearly supports the presented findings (Fig. 5). The Al spiking into the SCR of the 110 Ω/sq emitter results, on the one hand, in a rise of the *FF* loss due to R_{shunt} from $\Delta FF_{Rshunt} = 0.002\%_{abs}$ (35 Ω/sq) to $\Delta FF_{Rshunt} = 0.030\%_{abs}$ (110 Ω/sq$^{(b)}$). These figures, however, are within determination uncertainty. Hence, ΔFF_{Rshunt} has no considerable impact upon the fill factor. The major Al spiking induced *FF* loss, on the other hand, results from a growth of the recombination losses with ideality factor $n \neq 1$ in the SCR from $\Delta FF_{j02} = 1.97\%_{abs}$ (35 Ω/sq) to $\Delta FF_{j02} = 3.11\%_{abs}$ (110 Ω/sq$^{(b)}$). Still the greatest share of the total *FF* loss is based on R_{series} and amounts to $\Delta FF_{Rseries} = 3.78\text{-}3.99\%_{abs}$.

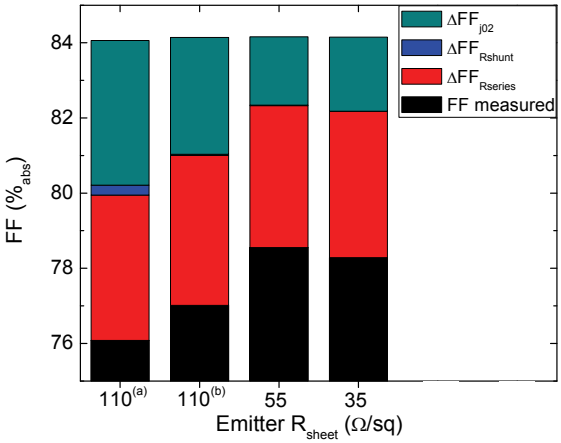

Fig. 5. Composition of *FF* losses according to FFLA.

For a more detailed investigation of the main loss origin, $\Delta FF_{Rseries}$ is itemized into all its components. Here, the greatest share is represented by the contributions from lateral conductivity within the etched-back FSF amounting to 1.5%$_{abs}$ for all samples. The remaining $\Delta FF_{Rseries}$ is mainly composed of contributions from the rear Al layer, Ag finger grid and front contact.

By varying R_{sheet} of the emitter, only the $\Delta FF_{Rseries}$ contributions of lateral conductivity within the emitter (ΔFF_{LC}) and the contact resistance (ΔFF_{CR}) to the rear metal are influenced. ΔFF_{LC} grows by only 0.02%$_{abs}$ to 0.03%$_{abs}$ when raising emitter sheet resistance from 35 to 110 Ω/sq$^{(b)}$. As this increase is also within determination uncertainty, the pitch of the contact holes on the rear is chosen short enough and thus, no significant impairment of *FF* due to lateral conductivity of the charge carriers within all three emitters towards the rear contact spots occurs.

However, enlarging the contact pitch for the benefit of reduced recombination would also increase contact resistance and therefore the $FF_{Rseries}$ loss. To calculate ΔFF_{CR}, the specific contact resistivity ρc of the three emitters needs to be known but can only be determined properly without the influence of laser ablation [10]. This process influences the emitter profile within a depth of ~100 nm. The ECV-measured surface concentration (not solely boron but also positively charged defects) increases by approximately 1.5 to 2 orders of magnitude generating a selective emitter structure [18]. This diminishes the specific contact resistivity compared to a non-laser-treated emitter by about one order of magnitude [19]. For a good approximation of ΔFF_{CR}, the emitter contact resistance contribution to R_{series} is calculated by subtracting all

remaining R_{series} contributions from the total R_{series} which results in ΔFF_{CR} values of 0.33 to 0.47%$_{abs}$. Considering the accumulated uncertainties for calculating the remaining individual R_{series} contributions and the total R_{series}, ΔFF_{CR} does virtually not depend on R_{sheet}.

Apart from the differences in lateral conductivity and contact resistivity, the observed $FF_{Rseries}$ disparities for the different R_{sheet} are rather attributed to process deviations as the laser-opened rear contact area (due to inhomogeneous SiN_x thickness) as well as the sinter temperature and duration. This is indicated by means of the two similarly processed 110 Ω/sq solar cells (a & b in Fig. 5) which also differ in the R_{series}-induced FF loss ($\Delta FF_{Rseries} = 0.12\%_{abs}$). An intensified annealing effect or a larger contact area reduces $\Delta FF_{Rseries}$ of the 110 Ω/sq$^{(a)}$ solar cell compared to its counterpart. On the other hand, it considerably increases ΔFF_{Rshunt} and ΔFF_{j02}, resulting in a 1%$_{abs}$ lower FF compared to its counterpart 110 Ω/sq$^{(b)}$.

Finally, the validity of the presented FFLA results is confirmed by comparing the sum of the measured FF and ΔFF_{series} from the FFLA (82.2%) with the pseudo fill factor pFF determined by the Suns-V_{OC} method (82.1%) (35 Ω/sq) proving nearly identical.

V. Summary

Within the European "20plµs" project, the entire production chain from wafering to module integration based on a mass-production compatible high-yield process for thin solar cells has been developed. For the first time, >20% efficient 80 µm thin large-area solar cells which have arisen from 100 µm wire-sawn c-Si wafers have been presented in this context.

A detailed fill factor analysis has identified differing recombination losses in the space charge region due to Al spiking to be predominantly responsible for the FF disparities of the solar cells with different emitter sheet resistances. For similarly processed solar cells, the variation of V_{OC}, FF and therefore η growing along with R_{sheet} is caused by recombination losses as well, but resulting from process fluctuations. The shallower the emitter, the higher is the impact of such process fluctuations. The greatest share of the total FF loss independent from R_{sheet} is based on R_{series} which is, for the larger part, caused by the contribution of lateral conductivity within the etched-back front surface field.

Thus, further improvements of the presented solar cell's performance can be accomplished primarily by selecting an appropriate emitter and reducing recombination in the SCR due to Al spiking as well as by reducing series resistance through an optimized ratio of front R_{sheet} and finger contact pitch.

Acknowledgement

The authors would like to thank Marcel Hofstetter for processing assistance and Bernd Weber for fruitful discussions concerning thin wafer sawing. The financial support for part of this work by the European Commission under FP7, contract number 256695 for the collaborative project "20 percent efficiency on less than 100 µm thick industrially feasible c-Si solar cells" (20plµs) is gratefully acknowledged.

The authors are solely responsible for this information and it does not represent the opinion of the European Community. The European Community is not responsible for any use that might be made of the data appearing therein.

References

[1] A. Goodrich, P. Hacke, Q. Wang, B. Sopori, R. Margolis, T. L. James, and M. Woodhouse, "A wafer-based monocrystalline silicon photovoltaics road map: Utilizing known technology improvement opportunities for further reductions in manufacturing costs," *Solar Energy Materials and Solar Cells*, vol. 114, pp. 110-135, 2013.

[2] M. Taguchi, Y. Tsunomura, H. Inoue, S. Taira, T. Nakashima, T. Baba, H. Sakata, and E. Maruyama, "High-efficiency HIT solar cell on thin (<100 µm) silicon wafer", in *24th European Photovoltaic Solar Energy Conference*, 2009, p. 1690.

[3] M. Taguchi, A. Yano, S. Tohoda, K. Matsuyama, Y. Nakamura, T. Nishiwaki, K. Fujita, and E. Maruyama, "24.7% record efficiency HIT solar cell on thin silicon wafer," *IEEE Journal of Photovoltaics*, vol. 4, pp. 96-99, 2014.

[4] P. Kapur, M. Moslehi, A. Deshpande, V. Rana, J. Kramer, S. Seutter, H. Deshazer, S. Coutant, A. Calcaterra, S. Kommera, Y.-S. Su, D. Grupp, S. Tamilmani, D. Dutton, T. Stalcup, T. Du, and M. Wingert, "A manufacturable, non-plated, non-Ag metallization based 20.44% efficient, 243cm^2 area, back contacted solar cell on 40um thick mono-crystalline silicon," in *28th European Photovoltaic Solar Energy Conference*, 2013, p. 2228.

[5] *International Technology Roadmap for Photovoltaic (ITRPV)*, 5th Edition, 2013 Results, 2014.

[6] B. Terheiden, T. Ballmann, R. Horbelt, Y. Schiele, S. Seren, J. Ebser, G. Hahn, V. Mertens, M. B. Koentopp et al., "Manufacturing 100-µm-thick silicon solar cells with efficiencies greater than 20% in a pilot production line," *Physica Status Solidi A*, vol. 212, pp. 13-24, 2015.

[7] G. Hahn, and A. Schönecker, "New crystalline silicon ribbon materials for photovoltaics," *Journal of Physics: Condensed Matter*, vol. 16, pp. R1615-R1648, 2004.

[8] B. Weber, S. Riepe, and H. J. Möller, "Increasing cutting efficiency of slurry based sawing process by use of structured wire," in *29th European Photovoltaic Solar Energy Conference*, 2014, p. 583.

[9] Y. Schiele, F. Book, S. Seren, G. Hahn, and B. Terheiden, "Screen-printed Al-alloyed rear junction solar cell concept applied to very thin (100 µm) large-area n-type Si wafers," *Energy Procedia*, vol. 27, pp. 460-466, 2012.

[10] Y. Schiele, S. Joos, G. Hahn, and B. Terheiden, "Etch-back of p^+ structures for selective boron emitters in n-type c-Si solar cells," *Energy Procedia*, vol. 55, pp. 295-301, 2014.

[11] Z. C. Holman, A. Descoeudres, S. De Wolf, and C. Ballif, "Record infrared internal quantum efficiency in silicon

heterojunction solar cells with dielectric/metal rear reflectors," *IEEE Journal of Photovoltaics*, vol. 3, pp. 1243-1249, 2013.

[12] T. Lauermann, T. Lüder, S. Scholz, B. Raabe, G. Hahn, and B. Terheiden, "Enabling dielectric rear side passivation for industrial mass production by developing lean printing-based solar cell processes," in *35th IEEE Photovoltaic Specialist Conference*, 2010, p. 28.

[13] H. Haverkamp, A. Dastgheib-Shirazi, B. Raabe, F. Book, and G. Hahn, "Minimizing the electrical losses on the front side: Development of a selective emitter process from a single diffusion, in *33rd IEEE Photovoltaic Specialist Conference*, 2008, p. 1.

[14] T. Lauermann, A. Dastgheib-Shirazi, F. Book, B. Raabe, G. Hahn, H. Haverkamp, D. Habermann, C. Demberger, and C. Schmid, "InSECT: An inline selective emitter concept with high efficiencies at competitive process costs improved with inkjet masking technology," in *24th European Photovoltaic Solar Energy Conference*, 2009, p. 1767.

[15] Y. Schiele, G. Hahn, and B. Terheiden, "Investigation of radiation damage to the Al_2O_3 / Si wafer interface during electron beam evaporation by means of C-V and lifetime measurements," in *26th European Photovoltaic Solar Energy Conference*, 2011, p. 1068.

[16] Y. Schiele, G. Hahn, and B. Terheiden, "Contacting and recombination analysis of boron emitters via etch-back for advanced n-type Si solar cells," in *29th European Photovoltaic Solar Energy Conference*, 2014, p. 825.

[17] A. Khanna, T. Müller, R. A. Stangl, B. Hoex, P. K. Basu, and A. G. Aberle, "A fill factor loss analysis method for silicon wafer solar cells," *IEEE Journal of Photovoltaics*, vol. 3, pp. 1170-1177, 2014.

[18] J. Engelhardt, *Schadenfreies Ablatieren von dielektrischen Schichten auf kristallinen Silizium-Scheiben*, Master Thesis, University of Konstanz, Konstanz, 2012.

[19] D. Pramanik, and A. N. Saxena, "VLSI metallization using aluminum and its alloys," Part 1, *Solid State Technology*, vol. 26, pp. 127-133, 1983.